Energy Storage Materials 13 (2018) 233–240

Contents lists available at ScienceDirect

Energy Storage Materials

journal homepage: www.elsevier.com/locate/ensm

Stretchable tandem micro-supercapacitors with high voltage output and exceptional mechanical robustness

Han Xiao[a], Zhong-Shuai Wu[a,*], Feng Zhou[a], Shuanghao Zheng[a,c,d], Dong Sui[b], Yongsheng Chen[b,*], Xinhe Bao[c]

[a] Dalian National Laboratory for Clean Energy, Dalian Institute of Chemical Physics, Chinese Academy of Sciences, 457 Zhongshan Road, Dalian 116023, PR China
[b] State Key Laboratory of Elemento-Organic Chemistry, Centre of Nanoscale Science and Technology and Key Laboratory of Functional Polymer Materials, College of Chemistry, Nankai University, Tianjin 300071, PR China
[c] State Key Laboratory of Catalysis, Dalian Institute of Chemical Physics, Chinese Academy of Sciences, 457 Zhongshan Road, Dalian 116023, PR China
[d] University of Chinese Academy of Sciences, 19 A Yuquan Road, Shijingshan District, Beijing 100049, PR China

ARTICLE INFO

Keywords:
Graphene
Stretchable
Tandem
Micro-supercapacitors
Energy storage

ABSTRACT

The drastic advancements in wearable electronics have ultimately stimulated the urgent development of stretchable microscale power sources with high voltage output and unprecedented integration. However, the creation of such energy storage devices remains elusive. Here we demonstrated the fabrication of stretchable tandem planar micro-supercapacitors (MSCs) with high voltage output, outstanding flexibility, robust cyclability, and sturdy integration, based on the interdigital electrode patterns of acid-treated, tightly intertwined graphene/carbon nanotube/cross-linked PH1000 film (GCP), in which PH1000 wrapped carbon nanotubes act as the stretchable backbone and capacitance contributor, and graphene nanosheets serve as high-conductive enhancer. The stretchable GCP patterns were directly manufactured by mask-assisted filtration of GCP ink, and transferred onto a pre-strain rubber substrate, showing high electrical conductivity (610 S cm^{-1}), and impressive stretchablitiy. The resultant GCP-MSCs delivered high areal capacitance of 107.5 mF cm^{-2}, and presented notable performance uniformity without obvious capacitance degradation after being stretched up to 200%, and stable cyclability with capacitance retention of 93.2% after 8000 cycles under repeatedly stretch-and-release strain. Moreover, our fabrication strategy is highly scalable for the generation of stretchable tandem MSCs without requirement of additional metal-based interconnects. As demonstrated, our stretchable tandem device of three serially-interconnected GCP-MSCs showed fully stretchable with strain rate up to 200%, and extended voltage output to 2.4 V in comparison with single cell (0.8 V), demonstrative of the great potential for wearable electronics.

1. Introduction

The ever-growing development for electronic textiles [1–3], electronic skins [4–6], and wearable health monitors [7,8] urgently calls for the stretchable microscale energy storage devices that can be compatibly bent, folded, twisted, and stretched while keep their electrochemical functions under deformation [9–15]. Stretchable supercapacitors have opened a new paradigm of application in stretchable electronics due to their high power density, long cyclability, and high-frequency response. So far, great advancements of stretchable supercapacitors have been achieved using the pre-designed electrode configurations, such as wrinkle macro-structure [16–18], interconnected bridge-island structure [19,20], honeycomb kirigami [21,22], and textile fiber structure [23–25]. However, developing stretchable supercapacitors is still facing tremendous challenges. First, the complicated steps of fabricating pre-designed substrates are often involved, such as deposition of conductive materials (e.g., Ag nanowires, carbon nanotubes) on elastic substrates [26–30], 3D printing [31], UV light exposure [32], photolithography [33], and gold coating [34]. Second, conventional inorganic materials with limited mechanical deformation and intrinsic polymers with poor conductivity suffer from low stretchablitiy and rate performance. Third, stretchable supercapacitors based on two stacked substrates are not suitable for integration in wearable electronics due to the severe interfacial mismatches of electrode, separator and electrolyte during deformation, resulting in significant performance degradation during skin and joint movement. Last but not

* Corresponding authors.
E-mail addresses: wuzs@dicp.ac.cn (Z.-S. Wu), yschen99@nankai.edu.cn (Y. Chen).

https://doi.org/10.1016/j.ensm.2018.01.019
Received 28 November 2017; Received in revised form 23 January 2018; Accepted 31 January 2018
Available online 02 February 2018

least, the usage of two substrates would intrinsically degrade the cell volumetric and gravimetric capacitances, and moreover, negatively impact the extended stretchability and integration of multiple cells.

Recently, micro-supercapacitors (MSCs), constructed with co-planar positive and negative electrodes separated by a narrow empty interspace on single substrate, have spurred intensive attention [35–42]. The key superiority of planar MSCs over stacked supercapacitors lies in exceptional interface match, outstanding shape diversification, and perfect integration of wearable electronics on single substrate. Despite huge progress of engineering high-performance electrode materials of nanocarbons (activated carbon [43,44], carbide-derived carbon [45], onion-like carbon [46], carbon nanotubes [47], and graphene [48–53]), metal oxides (e.g., RuO_2 [54], MnO_2 [55,56], CoO [57,58]), conducting polymers (e.g., polypyrrole [59], thiophene [60]) for MSCs, the innovative creation of stretchable tandem MSCs, featuring high voltage output and robust flexibility, are still not fully exploited. This is because that the fabrication of such multifunctional tandem devices needs to overcome some rather challenging intractable obstacles involving simultaneously such as engineering pre-designed microelectrodes, conducting stretchable interconnects and current collectors, mechanically reinforced electrolyte-integrated electrode and its interfacial adhesion to the stretchable substrate.

Herein, we developed a new type of highly stretchable tandem planar MSCs with metal-free interconnects and current collectors, exhibiting high voltage output, outstanding mechanical robustness, excellent cycling stability, and sturdy integration. The individual stretchable MSCs was manufactured based on the tightly intertwined, interdigital electrode patterns of acid-treated electrochemically exfoliated graphene (EG)/carbon nanotube (CNT)/poly (3,4-ethylenedioxythiophene):poly-(4-styrenesulfonate) (PEDOT:PSS, or PH1000) film (GCP) on an elastic pre-strained rubber substrate, covering gel electrolyte of poly(vinyl alcohol) (PVA)/H_3PO_4. The interdigital GCP microelectrodes were fabricated by mask-assisted deposition technique, in which cross-linked PH1000 (PH1000-CL) wrapped CNTs act as the stretchable backbone and capacitance contributor, EG nanosheets as conductive enhancer, and PH1000-CL as conducting network to intertwine CNTs and EG, allowing for the formation of stretchable, conducting and compact film. The as-obtained GCP films showed large electrical conductivity (610 S cm^{-1}), and outstanding stretchablitiy (up to 200%), and were directly employed as the binder- and additive-free electrodes for GCP-MSCs. Notably, GCP-MSCs presented high areal capacitance of 107.5 mF cm^{-2}, large stretchability up to 200% without obvious degradation of electrochemical performance, and remarkable cycling stability with 93.2% capacitance retention after 8000 cycles under repeated tensile strain. Moreover, our fabrication strategy is highly scalable for the production of fully stretchable tandem MSCs with strain rate up to 200%, showing the extended voltage output of 2.4 V for three serially-interconnected devices in comparison with single cell (200% strain, 0.8 V).

2. Experimental

2.1. Preparation of GCP dispersion

The GCP dispersion was obtained by mixing EG nanosheets, CNTs and PH1000 in ethanol/deionized water (1:1 vol%), and treated by tip sonication for 1 h. The concentration for each component is 0.1 mg mL^{-1}. Similarly, the CP (or GP) dispersion, containing 0.1 mg mL^{-1} for each CNTs (or EG) and PH1000, was prepared in ethanol/deionized water (1:1 vol%).

2.2. Fabrication of GCP-MSCs

Typically, 8 mL dispersion of GCP (CP, GP) was vacuum filtered through a polytetrafluoroethylene (PTFE) membrane (pore size 0.22 μm), and followed by the deposition of 2 mL 0.5 M H_2SO_4, with assistance of a customized interdigital mask with four fingers (lengths of 14 mm, widths of 1 mm, interspaces widths of 1 mm) on each side. Subsequently, the rubber substrate was pre-stretched with a strain rate of 230% and brushed by a thin-layer PVA aqueous solution (10 wt%). Then, the interdigital GCP (CP, GP) patterns were directly dry-transferred onto the pre-stretched rubber substrate. Note that the stretchable tandem GCP-MSCs were interconnected by a multi-step transferring process. The interconnects and contacts were realized by direct overlapping the end of GCP electrodes of bipolar cells during the transfer of GCP microelectrodes from PTFE membrane to pre-stretched rubber substrate. Finally, the gel electrolyte of PVA (Mw: 67000)/H_3PO_4 was drop-casted on the project area of microelectrodes.

2.3. Materials characterization

The morphology and structure of EG, CNTs, PH1000-CL and as-fabricated films (GCP, CP, GP) were characterized by scanning electron microscopy (SEM, JSM-7800F), transmission electron microscopy (TEM, JEM-2100), Raman spectrometer (LabRAM HR800), Attenuated total reflection Fourier transform infrared (ATR-FTIR, HYPERION 3000). The thickness of the films was examined by surface profiler (Veeco Dektak 150). Electrical conductivity of the films was measured by a standard four-point probe system (RTS-9).

2.4. Electrochemical characterization

Cyclic voltammetry (CV) curves tested at different scan rates of 5–2000 mV s^{-1}, galvanostatic charge and discharge (GCD) profiles measured at different current densities, and electrochemical impedance spectra (EIS) recorded in the frequency range of 0.01–100 kHz with a 5 mV AC amplitude were performed by CHI760E electrochemical workstation.

3. Results and discussion

The fabrication of stretchable tandem GCP-MSCs is schematically illustrated in Fig. 1. First, the solution-processable GCP dispersion of mixing high conducting EG nanosheets, multi-walled CNTs, and PH1000 was obtained by sonication in water/ethanol solvent (Fig. 1a). It is noted that EG nanosheets were directly synthesized from graphite by electrochemical cathodic exfoliation, and possessed exceptional electrical conductivity (> 1000 S cm^{-1}), which is suitable for boosting electrical conductivity of GCP film. In parallel, multi-walled CNTs, with lengths of tens of micrometers (Fig. S1, Supporting information), were chosen to enhance the mechanical robustness and capacitance of GCP film. The presence of PH1000 could well improve the stable dispersion of hydrophobic EG and CNTs (Fig. S2), and further served as effective flexible and conductive branches to boost mechanical robustness and electrical conductivity of GCP film through the intimate interfacial interaction with EG and CNTs (Fig. S3). Second, the resultant GCP dispersion (0.1 mg mL^{-1} for each component, 8 mL) was filtered through a PTFE membrane, with assistance of a customized interdigital mask, to form a shape-designable hybrid film (Fig. 1b, See details in Methods). Subsequently, the gelation agent of H_2SO_4 (0.5 M in water, 2 mL) was immediately filtrated, which is crucial for cross-linking of PH1000 component, resulting in conductive and elastic framework in GCP film [61]. ATR-FTIR spectra of GCP film, EG, CNTs, and PH1000-CL were compared in Fig. 2a. Apparently, no bands from EG and CNTs were observable, indicative of high quality nature with little oxygen-contain groups. The pronounced peaks of GCP film at 1160, 1120, 1060, and 1010 cm^{-1} were mainly assigned to the characteristic stretching vibrations of benzene sulfonate, and the band appeared at 1417 cm^{-1} was attributed to the –C=C– stretching vibration of aromatic rings, which are resulted from PH1000-CL component

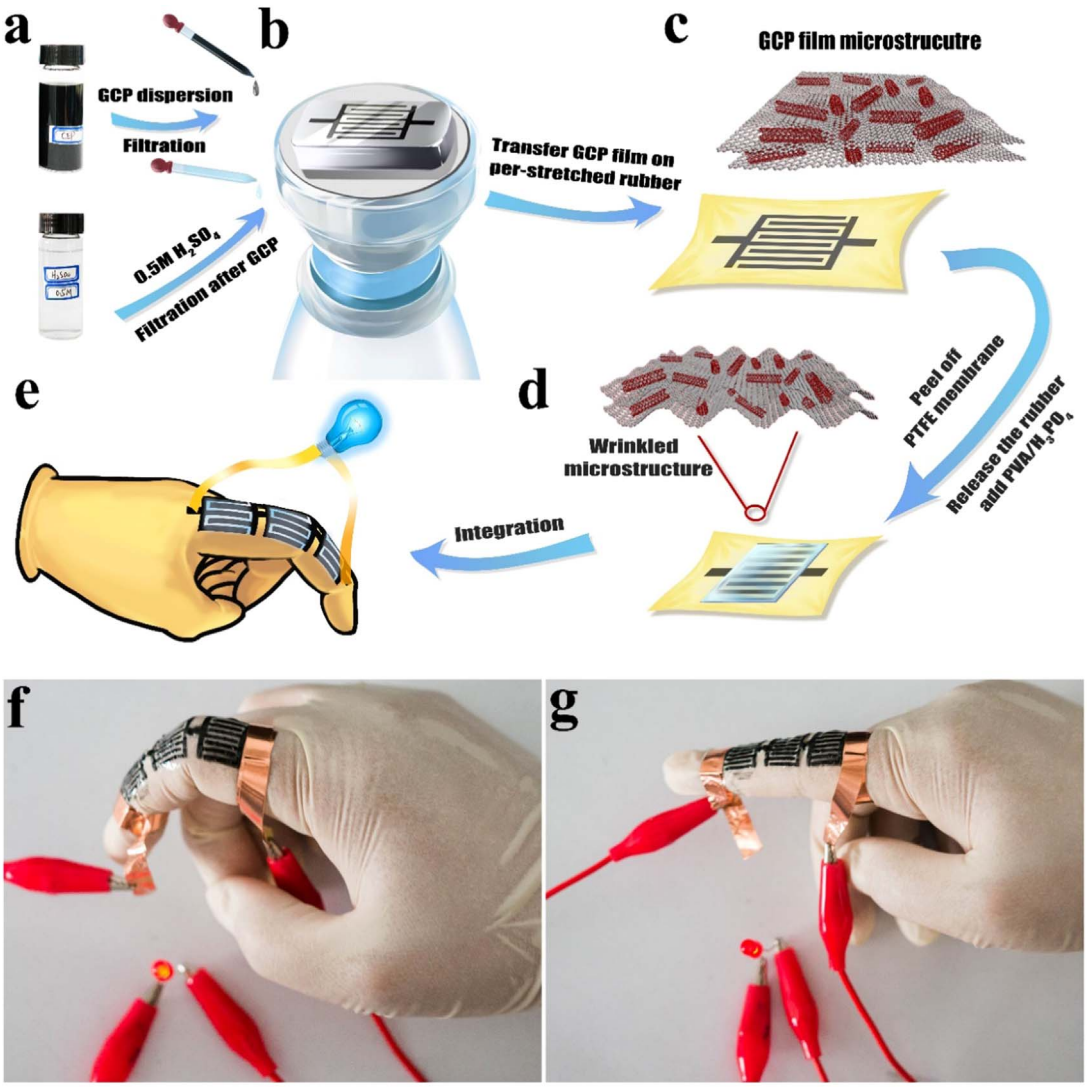

Fig. 1. Schematic of the fabrication and integration of GCP-MSCs. (a–e) The fabrication of GCP-MSCs, involving the steps of (a) preparation of GCP ink, (b) mask-assisted filtration of GCP ink and 0.5 M H_2SO_4 in sequence, (c) dry transfer of GCP interdigital patterns onto a pre-stretched rubber substrate, (d) peeling off PTFE membrane, and drop-casting electrolyte, (e) serial integration of GCP-MSCs on rubber glove. (f, g) Demonstration of stretchable tandem GCP-MSCs directly manufactured on a rubber glove, working as a wearable and stretchable power source for a light-emitting diode (LED) under different strain states.

[62]. Raman spectra further validated high quality of EG, showing a weak D peak at 1350 cm^{-1} and a sharp G peak at 1530 cm^{-1} (Fig. 2b). The I_D/I_G ratio of EG was only 0.2, much lower than CNTs (1.136), originating from the defective and unordered microstructure nature of CNTs. The strong band at 1432 cm^{-1} was assigned to the stretching vibration of thiophene rings [63], showing a slight redshift in comparison with untreated PH1000 (1424 cm^{-1}, Fig. S4) [61].

Afterward, the as-deposited GCP microelectrodes were directly dry-transferred onto a rubber substrate (Fig. 1c). Then, the stretched substrate was naturally released to the original state, and the wrinkle-structured and stretchable GCP microelectrodes were readily shaped (Fig. 1d). Top-view SEM (Fig. 2c and Fig. S3) and cross-section SEM (Fig. 2d, e) images validated the formation of a tightly intertwined and dense microstructure of GCP film, with an average thickness of ~ 8 μm at a strain state of 200%, showing that the tiled CNTs were tightly anchored on EG nanosheets. TEM and high-resolution TEM (HRTEM, Fig. 2f) images confirmed the intimate contact of CNTs with EG linked by PH1000-CL wrapping. It is explained that the hydrophobic polymer chain of PH1000 could fully cover the CNTs and EG surface, and the polar hydrophilic part could interact with water to dissociate the CNTs and EG well [64], resulting in the formation of tightly intertwined, cross-linked GCP films after acid treatment. As a consequence, the obtained GCP films possessed of outstanding mechanical robustness. Finally, after coating PVA/H_3PO_4 gel electrolyte, the stretchable GCP-MSCs were achieved (Fig. 1d). It is worth noting that our fabrication strategy is highly scalable for the facile production of stretchable tandem MSCs by direct overlapping the end of GCP stretchable electrodes of bipolar cells (Fig. 1e), without requirement of metal-based interconnects and contacts. As a representative example, our three serially-connected GCP-MSCs could operate well as a full stretchable energy storage device with superior adhesion on the rubber glove, and no any external force-induced shape failure and dimensional disruption was observed, even at a joint bending and stretching state (Fig. 1f, g).

The electrochemical performance of GCP-MSCs was first examined by CV measurement at different scan rates from 5 to 2000 mV s^{-1} (Fig. 3a, b). To understand the crucial roles and key contributions of CNTs, EG, and PH1000-CL in GCP film, we further constructed the MSCs based on CNT/PH1000-CL (CP) film (denoted as CP-MSCs) and EG/PH1000-CL (GP) film (denoted as GP-MSCs, Fig. S5 and Fig. S6),

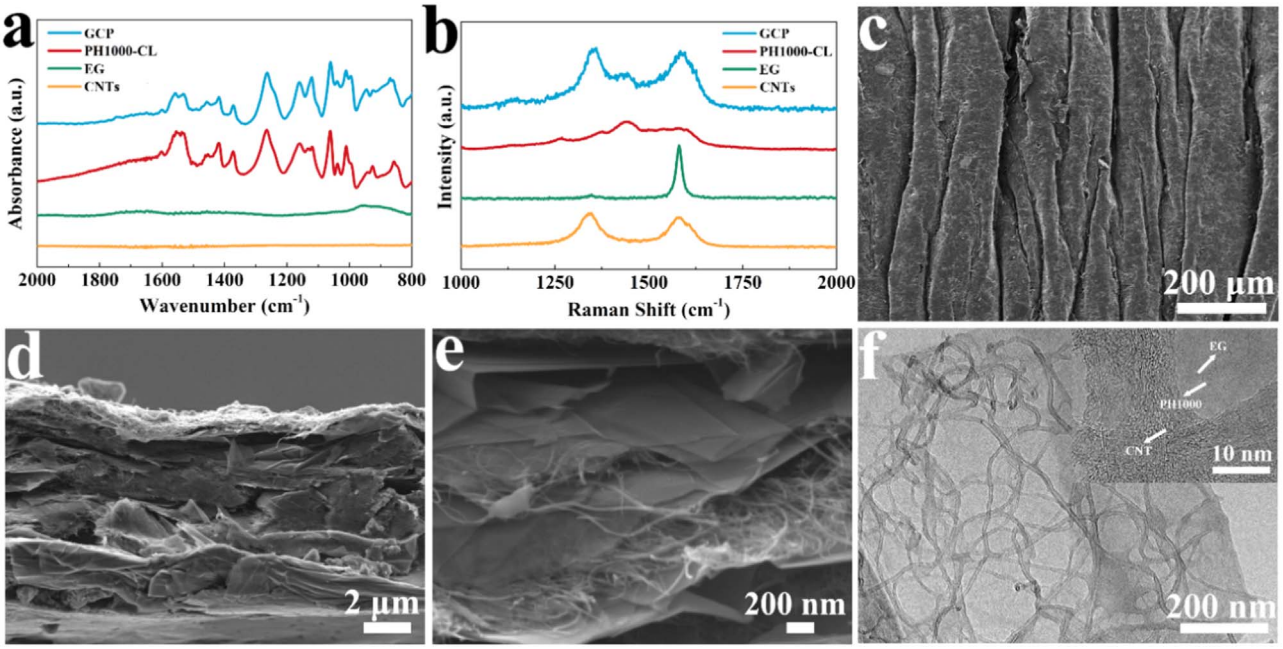

Fig. 2. Characterization of stretchable GCP microelectrodes. (a) ATR-FTIR and (b) Raman spectra of GCP film, PH1000-CL, EG, and CNTs, respectively. (c) Top-view SEM image of GCP microelectrode at a released state, showing a typical wrinkled microstructure. (d) Cross-section and (e) high-magnification SEM images of GCP microelectrode. (f) TEM image of GCP electrode. The inset is HRTEM of GCP, indicating that CNTs were tightly anchored on EG sheet by cross-linked PH1000.

while other steps were kept the same as GCP-MSCs. Note that GP-MSCs are not stretchable, due to the absence of CNTs, only for performance comparison (Fig. S7). After the optimization of areal capacitance and rate performance of GCP-MSCs (Fig. S8), we also chose 8 mL dispersion for the construction of CP-MSCs and GP-MSCs counterparts. The average film thickness for GCP-MSCs, CP-MSCs, and GP-MSCs evaluated by surface profiler were ~ 7.9, ~ 11.2, and ~ 4.9 μm, respectively (Fig. S9). Compared with CP film, the GCP film disclosed impressively decreased thickness due to the synergistic combination of tiled CNTs and large-size EG nanosheets with the anchored PH1000-CL, which significantly reduced the empty interspace caused by randomly distributed CNTs. As a result, the densely stacked GCP film presented much higher electrical conductivity of 610 S cm^{-1} than CP film (96 S cm^{-1}).

The CVs of GCP-MSCs exhibited a typical capacitive feature with a rectangular shape at low scan rates of 5–100 mV s^{-1}, illustrating the dominant behavior of electric double layer capacitors. Importantly, a significant capacitance contribution was observed up to 2000 mV s^{-1}, demonstrative of high ionic and electrical conductive networks in GCP film. The superior electrochemical performances of GCP-MSCs compared to CP-MSCs and GP-MSCs can be well elucidated by CV and GCD curves in Fig. 3c, d and Fig. S6. Apparently, the CV curves tested at 100 mV s^{-1} displayed more rectangular shape and larger areal integration, and GCD curves measured at 0.1 mA cm^{-2} represented nearly triangular symmetric shape and longer discharge time from GCP-MSCs, in comparison with CP-MSCs and GP-MSCs. The areal capacitances of GCP-MSCs, CP-MSCs, and GP-MSCs were given in Fig. 3e. Notably, GCP-MSCs and CP-MSCs, tested at 5 mV s^{-1}, delivered outstanding areal capacitance of 107.5 and 76.8 mF cm^{-2}, and volumetric capacitance of 45.3 and 22.9 F cm^{-3} at a released state, respectively. Both of them are much higher than those of GP-MSCs (0.7 mF cm^{-2} and 1.45 F cm^{-3} at 5 mV s^{-1}, Fig. S6). This value is much higher than those of the most reported stretchable supercapacitors (Table S1), such as graphene microribbons-MSCs (1 mF cm^{-2}) [34], CNT/Mn_3O_4-MSCs (2.2 mF cm^{-2}) [20], and nitrogen-doped CNT-MSCs (31.3 mF cm^{-2}) [65]. Further, high areal capacitances of ~ 15.2 mF cm^{-2} at 500 mV s^{-1} and ~ 4.4 mF cm^{-2} at a large scan rate of 2000 mV s^{-1} were still retained for GCP-MSCs. In a sharp contrast, lower capacitance, only ~ 1.8 mF cm^{-2} at 500 mV s^{-1}, was attained for CP-MSCs (Fig. S6), demonstrative of the importance of high conducting EG nanosheets. The enhanced rate capability of GCP-MCSs can be also confirmed by EIS (Fig. 3f), showing an equivalent series resistance (ESR) of ~ 64 Ω, while the ESR values are ~ 161 Ω for CP-MSCs and ~ 22 Ω for GP-MSCs. Remarkably, our GCP-MSCs represented a maximum areal energy density of ~ 1.27 μW h cm^{-2}, much higher than those of CP-MSCs (~ 0.91 μW h cm^{-2}) and GP-MSCs (~ 0.01 μW h cm^{-2}) (Fig. S10). Furthermore, GCP-MSCs delivered an impressive areal power density of ~ 1.22 mW cm^{-2} at energy density of ~ 0.54 μW h cm^{-2}.

To elucidate the outstanding mechanical stretchability, we used a homemade mechanical equipment to stretch our GCP-MSCs, and measured their electrochemical performance under different strain rates (Fig. 4). Fig. 4a–c illustrated the GCP-MSCs stretched at different strain rates of 0%, 100%, and 200%, respectively, and the insets represented the corresponding electrode structure evolution from highly wrinkled structure to the flat state. Of great importance is the unprecedented intimate contact of between GCP microelectrodes and the rubber substrate, in which neither the delamination of film from the substrate nor structural disruption was found at varying strain rates, even at strain rate of 200%. As expected, our GCP-MSCs demonstrated outstanding mechanical flexibility and electrochemical stability with high capacitance retention of 90% after 500 stretch-and-release cycles, and maintained a significant self-discharge time (Fig. S11). It is pointed out that H_2SO_4 acid treatment of PH1000 is very crucial for constructing a mechanically robust hydrogel of flexible PEDOT network [61], in which the CNTs were well intertwined together, and significantly buffer the deformation stress even under a slight overstretching state (Fig. S7 and S12). In a sharp contrast, if PH1000 in GCP film is not involved H_2SO_4 treatment, the capacitance of GCP-MSCs would drop fast during the repeated stretch-and-release cycles resulting from the poor mechanical flexibility of GCP film (Fig. S7 and S13). Furthermore, all the CV curves obtained at 100 mV s^{-1} and GCD curves measured at 0.1 mA cm^{-2} of GCP-MSCs were almost well overlapped when the device was stretched from the original state to

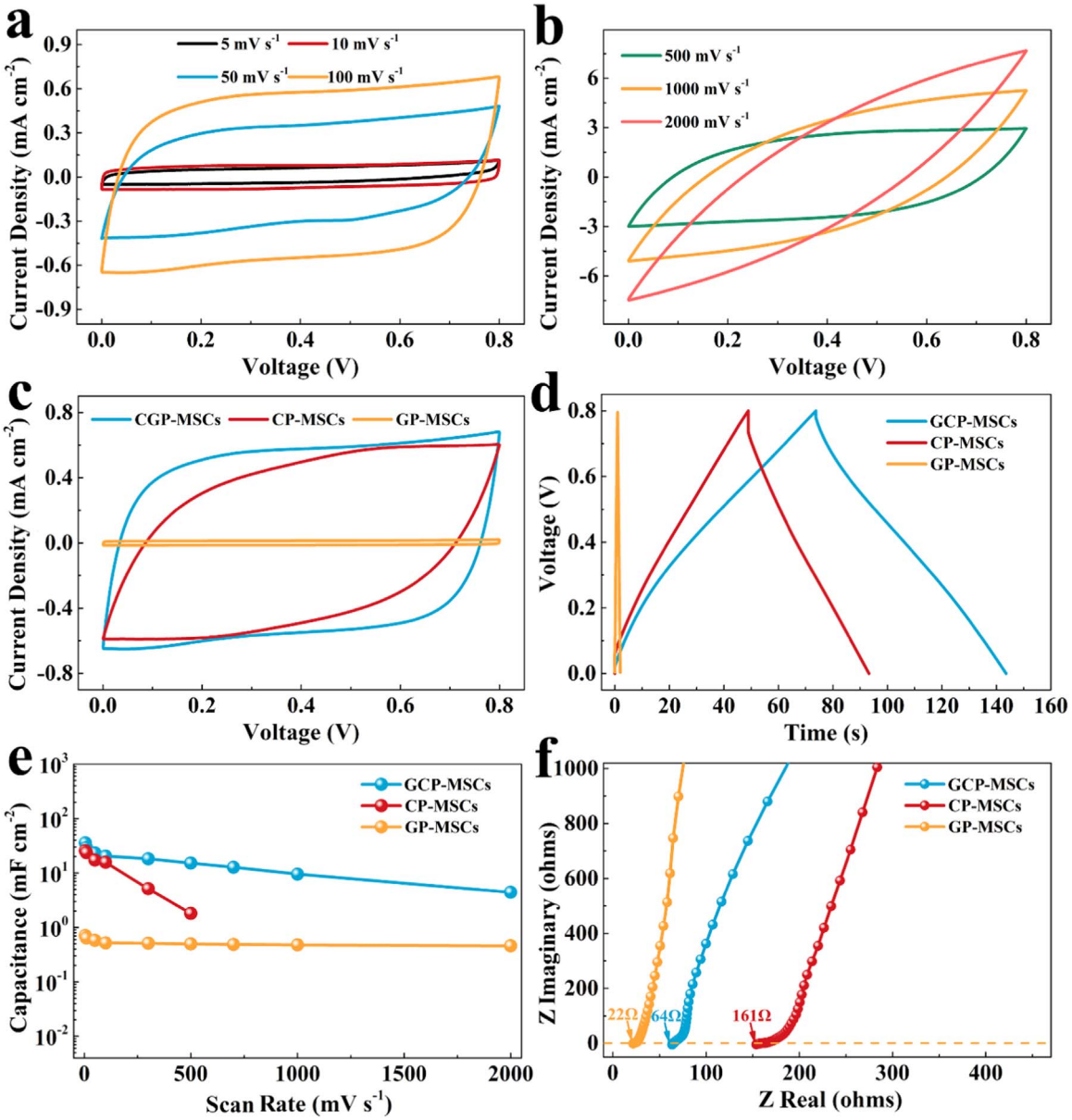

Fig. 3. Electrochemical characterization of GCP-MSCs, CP-MSCs (obtained at a strain rate of 200%), and GP-MSCs. (a, b) CV curves of GCP-MSCs obtained at different scan rates of (a) 5–100 mV s^{-1} and (b) 500–2000 mV s^{-1}. (c) CV curves of GCP-MSCs, CP-MSCs, and GP-MSCs measured at scan rate of 100 mV s^{-1}. (d) GCD curves of GCP-MSCs, CP-MSCs, and GP-MSCs obtained at current density of 0.1 mA cm^{-2}. (e) Areal capacitance of GCP-MSCs, CP-MSCs, and GP-MSCs as a function of scan rate. (f) The complex plane plot of GCP-MSCs, CP-MSCs, and GP-MSCs.

strain rate of 200% (Fig. 4d, e). In addition, the cycling stability of GCP-MSCs was measured at a current density of 0.5 mA cm^{-2}, testing 2000 cycles for each strain states from 200%, 100%, 0% to 200% (Fig. 4f). Impressively, after continuous 8000 cycles, 93.2% of initial capacitance for GCP-MSCs was still retained, suggestive of outstanding cyclability of our stretchable GCP-MSCs.

To further demonstrate the scalability and integration of our strategy, we adopted this approach to fabricate the stretchable tandem GCP-MSCs of integrating three serially-interconnected cells, without additional rigid metal connector, on a rubber substrate (Fig. 5). The resulting tandem GCP-MSCs exhibited a nearly rectangular CV shape (Fig. 5a) and closed to ideal symmetric triangular GCD curves (Fig. 5b), and the extended voltage of 2.4 V in comparison with single cell (0.8 V). Furthermore, the charge and discharge time of tandem GCP-MSCs tested at current density of 0.1 mA cm^{-2} are almost the same as single cell, representing high efficient integration of tandem GCP-MSCs. Moreover, both CV and GCD curves of stretchable tandem GCP-MSCs were almost overlapped well under different strain rates of 0%, 100% and 200% (Fig. 5c and Fig. S14), indicative of excellent performance uniformity and full stretchable properties. Notably, our tandem devices could easily power a LED when the integrated cell pack was stretched even at high strain rate of 200% (Fig. 5d), illustrating the great potential for stretchable electronics.

4. Conclusion

In summary, highly stretchable tandem GCP-MSCs capable of high voltage output, unprecedented mechanical robustness, superior integration, and applicable scalability were successfully fabricated based on the wrinkled micro-structured and robust interconnected GCP interdigital film. The as-fabricated GCP-MSCs showed high areal capacitance, outstanding rate capability, exceptional cyclability, and stable performance uniformity. Impressively, the stretchable tandem GCP-MSCs exhibited superior stretchability and electrochemical perfor-

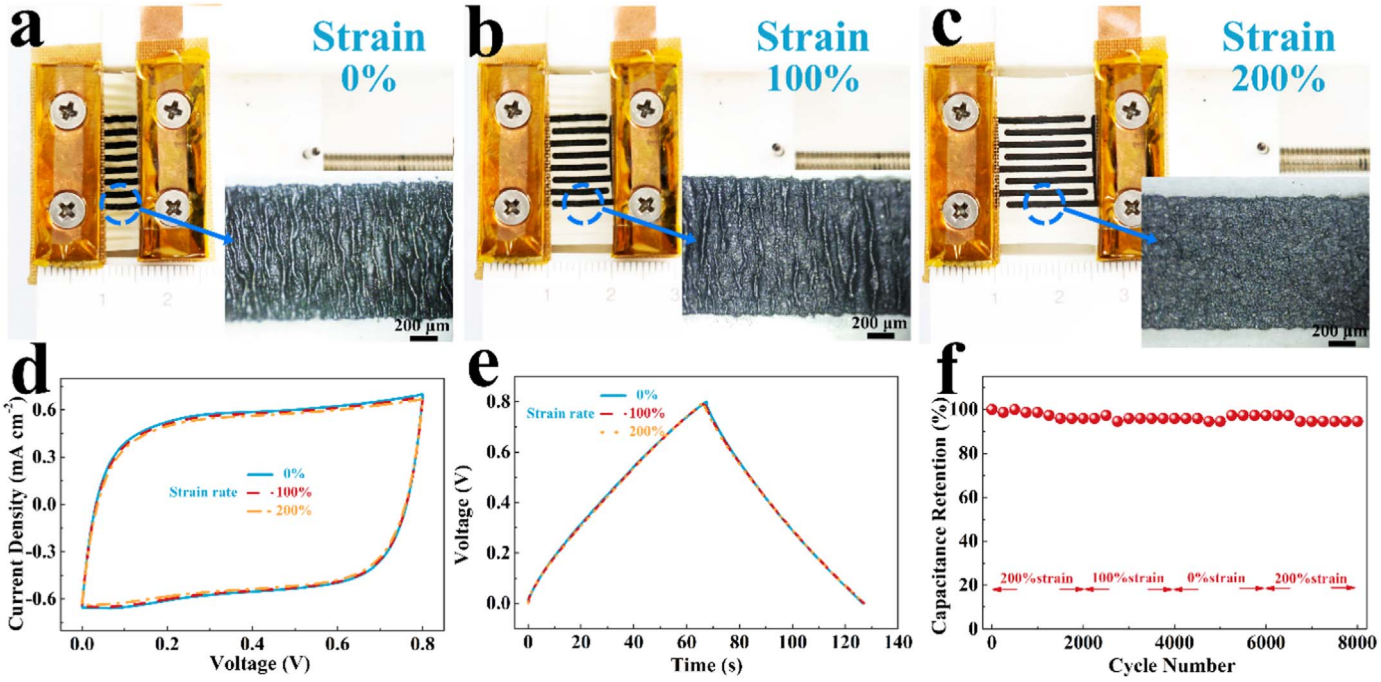

Fig. 4. Stretchability and cyclability of GCP-MSCs. (a–c) Photographs of GCP-MSCs tested at different strain rates of (a) 0%, (b) 100%, and (c) 200%. The insets are the corresponding optical images of microelectrodes. (d) CV curves of GCP-MSCs measured at 100 mV s^{-1}, and (e) GCD curves measured at 0.1 mA cm^{-2}, examined at different strain rates. (f) Cycling stability of GCP-MSCs obtained at 0.5 mA cm^{-2} for 8000 cycles under different strain states.

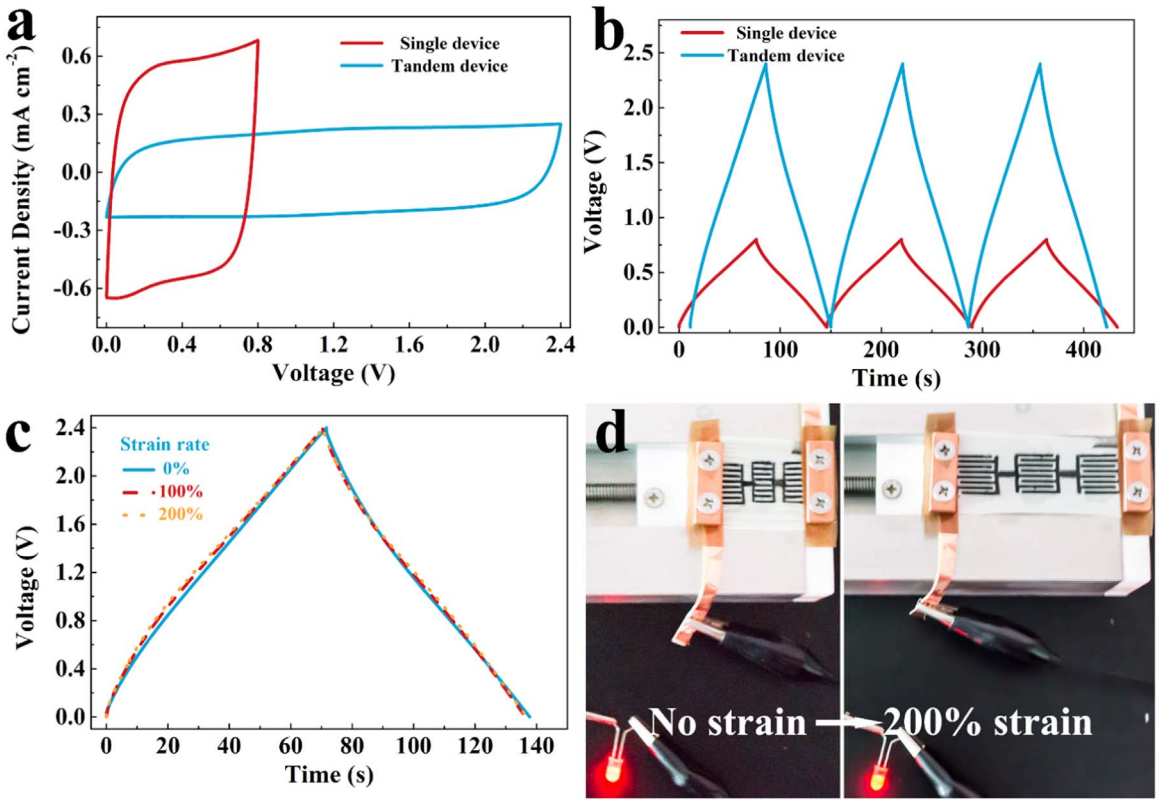

Fig. 5. Electrochemical performance of stretchable tandem GCP-MSCs interconnected by three cells. (a) CV curves obtained at 100 mV s^{-1}, and (b) GCD curves of stretchable tandem GCP-MSCs, tested at 0.1 mA cm^{-2}, under the strain state of 100%, in comparison with single device. (c) CV curves of stretchable tandem GCP-MSCs obtained at different strain rates, at 100 mV s^{-1}. (d) Photographs of stretchable tandem GCP-MSCs examined at the strain states of 0% (left) and 200% (right), both of which can easily power a LED.

mance, which rely on the synergistic combination of intertwined CNTs anchored on high conducting EG nanosheets by cross-linked PH1000, endowing the formation of high-conductive and elastic network for fast electron transport and rapid ion diffusion, and strong interfacial bonding of electrolyte/electrode/substrate. Compared to the most reported methods, e.g., photolithographic technique, for fabricating MSCs, our developed mask-assisted patterning approach is more convenient for manufacturing stretchable integrated MSCs, with high voltage output and remarkable mechanical robustness, as highly stretchable energy storage devices for wearable electronics.

Acknowledgements

This work was financially supported by the National Natural Science Foundation of China (Grants 51572259), National Key R & D Program of China (Grants 2016YFB0100100, and 2016YFA0200200), Natural Science Foundation of Liaoning Province (Grant 201602737), Recruitment Program of Global Expert (1000 Talent Plan), DICP (DICP ZZBS201708), China Postdoctoral Science Foundation (Grant 2016M601348), Exploratory Research Program of Shaanxi Yanchang Petroleum (Group) Co., LTD & DICP.

Appendix A. Supplementary material

Supplementary data associated with this article can be found in the online version at doi:10.1016/j.ensm.2018.01.019.

References

[1] N. Matsuhisa, M. Kaltenbrunner, T. Yokota, H. Jinno, K. Kuribara, T. Sekitani, T. Someya, Printable elastic conductors with a high conductivity for electronic textile applications, Nat. Commun. 6 (2015) 7461.
[2] Y. Liu, M. Pharr, G.A. Salvatore, Lab-on-skin: a review of flexible and stretchable electronics for wearable health monitoring, ACS Nano 11 (2017) 9614–9635.
[3] Y. Huang, H. Hu, Y. Huang, M.S. Zhu, W.J. Meng, C. Liu, Z.X. Pei, C.L. Hao, Z.K. Wang, C.Y. Zhi, From industrially weavable and knittable highly conductive yarns to large wearable energy storage textiles, ACS Nano 9 (2015) 4766–4775.
[4] C. Larson, B. Peele, S. Li, S. Robinson, M. Totaro, L. Beccai, B. Mazzolai, R. Shepherd, Highly stretchable electroluminescent skin for optical signaling and tactile sensing, Science 351 (2016) 1071–1074.
[5] A.J. Bandodkar, J.M. You, N.H. Kim, Y. Gu, R. Kumar, A.M.V. Mohan, J. Kurniawan, S. Imani, T. Nakagawa, B. Parish, M. Parthasarathy, P.P. Mercier, S. Xu, J. Wang, Soft, stretchable, high power density electronic skin-based biofuel cells for scavenging energy from human sweat, Energy Environ. Sci. 10 (2017) 1581–1589.
[6] S.C. Mannsfeld, B.C. Tee, R.M. Stoltenberg, C.V. Chen, S. Barman, B.V. Muir, A.N. Sokolov, C. Reese, Z. Bao, Highly sensitive flexible pressure sensors with microstructured rubber dielectric layers, Nat. Mater. 9 (2010) 859–864.
[7] J.Y. Oh, S. Rondeau-Gagne, Y.C. Chiu, A. Chortos, F. Lissel, G.N. Wang, B.C. Schroeder, T. Kurosawa, J. Lopez, T. Katsumata, J. Xu, C. Zhu, X. Gu, W.G. Bae, Y. Kim, L. Jin, J.W. Chung, J.B. Tok, Z. Bao, Intrinsically stretchable and healable semiconducting polymer for organic transistors, Nature 539 (2016) 411–415.
[8] Q. Liu, J. Chen, Y.R. Li, G.Q. Shi, High-performance strain sensors with fish-scale-like graphene-sensing layers for full-range detection of human motions, ACS Nano 10 (2016) 7901–7906.
[9] Z.F. Liu, S. Fang, F.A. Moura, J.N. Ding, N. Jiang, J. Di, M. Zhang, X. Lepro, D.S. Galvao, C.S. Haines, N.Y. Yuan, S.G. Yin, D.W. Lee, R. Wang, H.Y. Wang, W. Lv, C. Dong, R.C. Zhang, M.J. Chen, Q. Yin, Y.T. Chong, R. Zhang, X. Wang, M.D. Lima, R. Ovalle-Robles, D. Qian, H. Lu, R.H. Baughman, Hierarchically buckled sheath-core fibers for superelastic electronics, sensors, and muscles, Science 349 (2015) 400–404.
[10] D.Y. Khang, H. Jiang, Y. Huang, J.A. Rogers, A stretchable form of single-crystal silicon for high-performance electronics on rubber substrates, Science 311 (2006) 208–212.
[11] B.Y. Ahn, E.B. Duoss, M.J. Motala, X. Guo, S.I. Park, Y. Xiong, J. Yoon, R.G. Nuzzo, J.A. Rogers, J.A. Lewis, Omnidirectional printing of flexible, stretchable, and spanning silver microelectrodes, Science 323 (2009) 1590–1593.
[12] T. Cheng, Y. Zhang, W.Y. Lai, W. Huang, Stretchable thin-film electrodes for flexible electronics with high deformability and stretchability, Adv. Mater. 27 (2015) 3349–3376.
[13] F. Zhang, Y. Lu, X. Yang, L. Zhang, T. Zhang, K. Leng, Y. Wu, Y. Huang, Y. Ma, Y. Chen, A flexible and high-voltage internal tandem supercapacitor based on graphene-based porous materials with ultrahigh energy density, Small 10 (2014) 2285–2292.
[14] H. Xiao, Z.-S. Wu, L. Chen, F. Zhou, S. Zheng, W. Ren, H.M. Cheng, X. Bao, One-step device fabrication of phosphorene and graphene interdigital micro-supercapacitors with high energy density, ACS Nano 11 (2017) 7284–7292.
[15] S. Zheng, X. Tang, Z.-S. Wu, Y.Z. Tan, S. Wang, C. Sun, H.M. Cheng, X. Bao, Arbitrary-shaped graphene-based planar sandwich supercapacitors on one substrate with enhanced flexibility and integration, ACS Nano 11 (2017) 2171–2179.
[16] J.S. Xu, J. Chen, M. Zhang, J.D. Hong, G.Q. Shi, Highly conductive stretchable electrodes prepared by in situ reduction of wavy graphene oxide films coated on elastic tapes, Adv. Electron. Mater. 2 (2016) 1600022.
[17] J. Zang, C. Cao, Y. Feng, J. Liu, X. Zhao, Stretchable and high-performance supercapacitors with crumpled graphene papers, Sci. Rep. 4 (2014) 6492–6498.
[18] T. Chen, Y.H. Xue, A.K. Roy, L.M. Dai, Transparent and stretchable high-performance supercapacitors based on wrinkled graphene electrodes, ACS Nano 8 (2014) 1039–1046.
[19] Y. Lim, J. Yoon, J. Yun, D. Kim, S.Y. Hong, S.J. Lee, G. Zi, J.S. Ha, Biaxially stretchable, integrated array of high performance microsupercapacitors, ACS Nano 8 (2014) 11639–11650.
[20] G. Lee, D. Kim, D. Kim, S. Oh, J. Yun, J. Kim, S.S. Lee, J.S. Ha, Fabrication of a stretchable and patchable array of high performance micro-supercapacitors using a non-aqueous solvent based gel electrolyte, Energy Environ. Sci. 8 (2015) 1764–1774.
[21] J. Pu, X. Wang, R. Xu, K. Komvopoulos, Highly stretchable microsupercapacitor arrays with honeycomb structures for integrated wearable electronic systems, ACS Nano 10 (2016) 9306–9315.
[22] H. Guo, M.H. Yeh, Y.C. Lai, Y. Zi, C. Wu, Z. Wen, C. Hu, Z.L. Wang, All-in-one shape-adaptive self-charging power package for wearable electronics, ACS Nano 10 (2016) 10580–10588.
[23] Y. Meng, Y. Zhao, C. Hu, H. Cheng, Y. Hu, Z. Zhang, G. Shi, L. Qu, All-graphene core-sheath microfibers for all-solid-state, stretchable fibriform supercapacitors and wearable electronic textiles, Adv. Mater. 25 (2013) 2326–2331.
[24] Z. Yang, J. Deng, X. Chen, J. Ren, H. Peng, A highly stretchable, fiber-shaped supercapacitor, Angew. Chem. Int. Ed. 52 (2013) 13453–13457.
[25] F. Meng, Q. Li, L. Zheng, Flexible fiber-shaped supercapacitors: design, fabrication, and multi-functionalities, Energy Storage Mater. 8 (2017) 85–109.
[26] M. Yu, Y. Zhang, Y. Zeng, M.S. Balogun, K. Mai, Z. Zhang, X. Lu, Y. Tong, Water surface assisted synthesis of large-scale carbon nanotube film for high-performance and stretchable supercapacitors, Adv. Mater. 26 (2014) 4724–4729.
[27] F. Xu, Y. Zhu, Highly conductive and stretchable silver nanowire conductors, Adv. Mater. 24 (2012) 5117–5122.
[28] T. Chen, H. Peng, M. Durstock, L. Dai, High-performance transparent and stretchable all-solid supercapacitors based on highly aligned carbon nanotube sheets, Sci. Rep. 4 (2014) 3612–3618.
[29] X. Chen, H. Lin, P. Chen, G. Guan, J. Deng, H. Peng, Smart, stretchable supercapacitors, Adv. Mater. 26 (2014) 4444–4449.
[30] Z. Niu, H. Dong, B. Zhu, J. Li, H.H. Hng, W. Zhou, X. Chen, S. Xie, Highly stretchable, integrated supercapacitors based on single-walled carbon nanotube films with continuous reticulate architecture, Adv. Mater. 25 (2013) 1058–1064.
[31] L. Li, Z. Lou, W. Han, D. Chen, K. Jiang, G.Z. Shen, Highly stretchable micro-supercapacitor arrays with hybrid MWCNT/PANI electrodes, Adv. Mater. Technol. 2 (2017) 1600282.
[32] C. Yu, C. Masarapu, J. Rong, B. Wei, H. Jiang, Stretchable supercapacitors based on buckled single-walled carbon-nanotube macrofilms, Adv. Mater. 21 (2009) 4793–4797.
[33] D. Kim, G. Shin, Y.J. Kang, W. Kim, J.S. Ha, Fabrication of a stretchable solid-state micro-supercapacitor array, ACS Nano 7 (2013) 7975–7982.
[34] D. Qi, Z. Liu, Y. Liu, W.R. Leow, B. Zhu, H. Yang, J. Yu, W. Wang, H. Wang, S. Yin, X. Chen, Suspended wavy graphene microribbons for highly stretchable micro-supercapacitors, Adv. Mater. 27 (2015) 5559–5566.
[35] P. Simon, Y. Gogotsi, Materials for electrochemical capacitors, Nat. Mater. 7 (2008) 845–854.
[36] Y. Zhu, S. Murali, M.D. Stoller, K.J. Ganesh, W. Cai, P.J. Ferreira, A. Pirkle, R.M. Wallace, K.A. Cychosz, M. Thommes, D. Su, E.A. Stach, R.S. Ruoff, Carbon-based supercapacitors produced by activation of graphene, Science 332 (2011) 1537–1541.
[37] S. Zheng, Z.-S. Wu, S. Wang, H. Xiao, F. Zhou, C. Sun, X. Bao, H.-M. Cheng, Graphene-based materials for high-voltage and high-energy asymmetric super-capacitors, Energy Storage Mater. 6 (2017) 70–97.
[38] Z.-S. Wu, X.L. Feng, H.M. Cheng, Recent advances in graphene-based planar micro-supercapacitors for on-chip energy storage, Natl. Sci. Rev. 1 (2014) 277–292.
[39] Z.W. Peng, R.Q. Ye, J.A. Mann, D. Zakhidov, Y.L. Li, P.R. Smalley, J. Lin, J.M. Tour, Flexible boron-doped laser-induced graphene microsupercapacitors, ACS Nano 9 (2015) 5868–5875.
[40] J.B. Goodenough, Energy storage materials: a perspective, Energy Storage Mater. 1 (2015) 158–161.
[41] Z.-S. Wu, S. Yang, L. Zhang, J.B. Wagner, X. Feng, K. Müllen, Binder-free activated graphene compact films for all-solid-state micro-supercapacitors with high areal and volumetric capacitances, Energy Storage Mater. 1 (2015) 119–126.
[42] K. Guo, Y. Wan, N. Yu, L. Hu, T. Zhai, H. Li, Hand-drawing patterned ultra-thin integrated electrodes for flexible micro supercapacitors, Energy Storage Mater. 11 (2018) 144–151.
[43] L. Wei, N. Nitta, G. Yushin, Lithographically patterned thin activated carbon films as a new technology platform for on-chip devices, ACS Nano 7 (2013) 6498–6506.
[44] H.-C. Huang, C.-J. Chung, C.-T. Hsieh, P.-L. Kuo, H. Teng, Laser fabrication of all-solid-state microsupercapacitors with ultrahigh energy and power based on hierarchical pore carbon, Nano Energy 21 (2016) 90–105.
[45] J. Chmiola, C. Largeot, P.L. Taberna, P. Simon, Y. Gogotsi, Monolithic carbide-derived carbon films for micro-supercapacitors, Science 328 (2010) 480–483.

[46] D. Pech, M. Brunet, H. Durou, P.H. Huang, V. Mochalin, Y. Gogotsi, P.L. Taberna, P. Simon, Ultrahigh-power micrometre-sized supercapacitors based on onion-like carbon, Nat. Nanotechnol. 5 (2010) 651–654.
[47] S.K. Kim, H.J. Koo, A. Lee, P.V. Braun, Selective wetting-induced micro-electrode patterning for flexible micro-supercapacitors, Adv. Mater. 26 (2014) 5108–5112.
[48] W. Gao, N. Singh, L. Song, Z. Liu, A.L.M. Reddy, L.J. Ci, R. Vajtai, Q. Zhang, B.Q. Wei, P.M. Ajayan, Direct laser writing of micro-supercapacitors on hydrated graphite oxide films, Nat. Nanotechnol. 6 (2011) 496–500.
[49] Z.-S. Wu, K. Parvez, X.L. Feng, K. Müllen, Graphene-based in-plane micro-supercapacitors with high power and energy densities, Nat. Commun. 4 (2013) 2487.
[50] Z.K. Wu, Z.Y. Lin, L.Y. Li, B. Song, K.S. Moon, S.L. Bai, C.P. Wong, Flexible micro-supercapacitor based on in-situ assembled graphene on metal template at room temperature, Nano Energy 10 (2014) 222–228.
[51] H. Wu, Y. Zhang, L. Cheng, L. Zheng, Y. Li, W. Yuan, X. Yuan, Graphene based architectures for electrochemical capacitors, Energy Storage Mater. 5 (2016) 8–32.
[52] S. Zheng, W. Lei, J. Qin, Z.-S. Wu, F. Zhou, S. Wang, X. Shi, C. Sun, Y. Chen, X. Bao, All-solid-state high-energy planar asymmetric supercapacitors based on all-in-one monolithic film using boron nitride nanosheets as separator, Energy Storage Mater. 10 (2018) 24–31.
[53] Y.-Z. Liu, Y.-F. Li, F.-Y. Su, L.-J. Xie, Q.-Q. Kong, X.-M. Li, J.-G. Gao, C.-M. Chen, Easy one-step synthesis of N-doped graphene for supercapacitors, Energy Storage Mater. 2 (2016) 69–75.
[54] A. Ferris, S. Garbarino, D. Guay, D. Pech, 3D RuO_2 microsupercapacitors with remarkable areal energy, Adv. Mater. 27 (2015) 6625–6629.
[55] Z. Su, C. Yang, B. Xie, Z. Lin, Z. Zhang, J. Liu, B. Li, F. Kang, C.P. Wong, Scalable fabrication of MnO_2 nanostructure deposited on free-standing Ni nanocone arrays for ultrathin, flexible, high-performance microsupercapacitor, Energy Environ. Sci. 7 (2014) 2652–2659.
[56] H. Wang, C. Xu, Y. Chen, Y. Wang, MnO_2 nanograsses on porous carbon cloth for flexible solid-state asymmetric supercapacitors with high energy density, Energy Storage Mater. 8 (2017) 127–133.
[57] Y.G. Zhu, Y. Wang, Y. Shi, J.I. Wong, H.Y. Yang, CoO nanoflowers woven by CNT network for high energy density flexible micro-supercapacitor, Nano Energy 3 (2014) 46–54.
[58] S. Aloqayli, C.K. Ranaweera, Z. Wang, K. Siam, P.K. Kahol, P. Tripathi, O.N. Srivastava, B.K. Gupta, S.R. Mishra, F. Perez, X. Shen, R.K. Gupta, Nanostructured cobalt oxide and cobalt sulfide for flexible, high performance and durable supercapacitors, Energy Storage Mater. 8 (2017) 68–76.
[59] S. Liu, P. Gordiichuk, Z.-S. Wu, Z. Liu, W. Wei, M. Wagner, N. Mohamed-Noriega, D. Wu, Y. Mai, A. Herrmann, K. Müllen, X. Feng, Patterning two-dimensional free-standing surfaces with mesoporous conducting polymers, Nat. Commun. 6 (2015) 8817.
[60] Z.-S. Wu, Y. Zheng, S. Zheng, S. Wang, C. Sun, K. Parvez, T. Ikeda, X. Bao, K. Müllen, X. Feng, Stacked-layer heterostructure films of 2D thiophene nanosheets and graphene for high-rate all-solid-state pseudocapacitors with enhanced volumetric capacitance, Adv. Mater. 29 (2017) 1602960.
[61] B. Yao, H. Wang, Q. Zhou, M. Wu, M. Zhang, C. Li, G. Shi, Ultrahigh-conductivity polymer hydrogels with arbitrary structures, Adv. Mater. 29 (2017) 1700974.
[62] J. Ouyang, Q.F. Xu, C.W. Chu, Y. Yang, G. Li, J. Shinar, On the mechanism of conductivity enhancement in poly (3,4-ethylenedioxythiophene): poly(styrene sulfonate) film through solvent treatment, Polymer 45 (2004) 8443–8450.
[63] B.Y. Ouyang, C.W. Chi, F.C. Chen, Q.F. Xi, Y. Yang, High-conductivity poly (3,4-ethylenedioxythiophene): poly(styrene sulfonate) film and its application in polymer optoelectronic devices, Adv. Funct. Mater. 15 (2005) 203–208.
[64] Z. Chen, J.W.F. To, C. Wang, Z.D. Lu, N. Liu, A. Chortos, L.J. Pan, F. Wei, Y. Cui, Z.N. Bao, A three-dimensionally interconnected carbon nanotube-conducting polymer hydrogel network for high-performance flexible battery electrodes, Adv. Energy Mater. 4 (2014) 1400207.
[65] Z.T. Zhang, L. Wang, Y.M. Li, Y.H. Wang, J. Zhang, G.Z. Guan, Z.Y. Pan, G.F. Zheng, H.S. Peng, Nitrogen-doped core-sheath carbon nanotube array for highly stretchable supercapacitor, Adv. Energy Mater. 7 (2017) 1601814.